Further investigations of linear trirhodium complexes: experimental and theoretical studies of $[Rh_3(dpa)_4Cl_2]$ and $[Rh_3(dpa)_4Cl_2](BF_4)$ [dpa = bis(2-pyridyl)amido anion]†

Gin-Chen Huang,[a] Isiah Po-Chun Liu,‡[a,b] Jau-Huei Kuo,[a] Yi-Lin Huang,[c] Chen-Yu Yeh,[c] Gene-Hsiang Lee[a] and Shie-Ming Peng*[a,b]

Received 10th November 2008, Accepted 16th January 2009
First published as an Advance Article on the web 20th February 2009
DOI: 10.1039/b820060b

The linear trirhodium compound, $Rh_3(dpa)_4Cl_2$ (**1**), and its one-electron oxidation product, $[Rh_3(dpa)_4Cl_2]BF_4$ (**2**), have been synthesized and studied extensively. The magnetic measurement for compound **1** shows that it possesses one unpaired electron that is assigned to occupy the σ_{nb} orbital ($^2A_2$) by DFT calculations. Upon oxidation, a β-spin electron of **1** is removed, that causes compound **2** to exhibit a triplet ground state. DFT calculations indicate that the two unpaired electrons of **2** occupy σ_{nb} and δ* orbitals ($^3B_1$), which is supported by ^1H NMR spectrum. Unlike their isoelectronic analogues $[Co_3(dpa)_4Cl_2]$ (**3**) and $[Co_3(dpa)_4(Cl)_2]BF_4$ (**4**), both compound **1** and **2** do not display the spin-crossover phenomenon. The reason may be attributed to the relative large energy gap between $^3B_1$ and open-shell singlet $^1B_1$ states.

Introduction

Metal string complexes with a linear transition-metal framework are expected to serve as molecular wires and are potential materials for use in future nanoelectronic devices.[1] Because of this, over the last twenty years a number of tri-, tetra-, penta-, hexa-, hepta-, octa-, and nonanuclear metal string complexes with a first row transition metal backbone have been synthesized and characterized.[2] It is more difficult to synthesize metal string complexes containing heavier transition metals (4d or 5d) than their 3d transition metal analogues; therefore, in the past two decades the study of the metal string complexes has generally focused on the first transition series. Only a few attempts have been made to investigate metal string complexes with heavier transition metal ions.[3]

The greater orbital diffuseness and spin-orbital coupling of heavier transition metal ions may lead to various physical properties of the metal string complexes which are quite different from those of first row transition metals. It should be interesting to synthesize and study metal string complexes with heavier transition metal ions in view of the synthetic challenge and the fact that their physical and chemical properties remain unknown. To extend our studies to second row transition metal ions, we reported the synthesis and structures of the linear triruthenium and trirhodium complexes in 1996 and their yields were relatively low.[3a] Recently, the yield for the linear triruthenium compounds has been greatly improved under modified conditions and this allows us to obtain a large amount of material for further studies.[3b] The most remarkable behavior for the triruthenium complexes is that the electronic configuration changes significantly as the axial ligands are altered from chlorides to cyanides and this has never been observed in metal string complex with first row transition metal ions.[3b]

The interesting properties of the triruthenium complexes prompted us to further study the trirhodium analogues. In the present work, we report the synthesis, crystal structures, electrochemical and magnetic properties, and DFT calculations of the trirhodium compound, $[Rh_3(dpa)_4Cl_2]$ (**1**), and its one-electron oxidation product, $[Rh_3(dpa)_4Cl_2](BF_4)$ (**2**). In addition, the properties of **1** and **2** have been compared with those of the isoelectronic symmetric tricobalt compounds, $[Co_3(dpa)_4Cl_2]$ (**3**) and $[Co_3(dpa)_4Cl_2]BF_4$ (**4**).[4,5]

Results and discussion

Synthesis and crystal structures

Complex **1** was synthesized according to our previously reported method under modified conditions.[3a] By treating compound **1** with $FcBF_4$ (1.1 eq.) in CH_2Cl_2 and MeOH, the one-electron oxidized compound $[Rh_3(dpa)_4Cl_2][BF_4]$ (**2**) was obtained in good yield. Crystallization of this product from CH_2Cl_2 and hexane produced deep green crystals. Crystallographic data for **2** are given in Table 1.

Selected bond lengths and angles for **1** and **2** are summarized in Table 2. The crystal structure of **1**, has already been discussed in our previous report.[3a] The Rh–Rh–Rh chain of **1** is approximately linear (∠Rh(1)–Rh(2)–Rh(3) = 177.13°) and helically wrapped by four dpa^- ligands with two Cl^- as the axial ligands. Because of the formation of the metal–metal bond, the coordination environment of each Rh atom displays a distorted octahedral

[a]*Department of Chemistry, National Taiwan University, Taipei, Taiwan, (ROC)*
[b]*Institute of Chemistry, Academia Sinica, Nankang, Taipei, Taiwan, (ROC)*
[c]*Department of Chemistry, National Chung-Hsing University, Taichung, Taiwan, (ROC)*

† Electronic supplementary information (ESI) available: Computational results for **1** and **2** with different basis sets and functionals. CCDC reference number 708776 **2**. For ESI and crystallographic data in CIF or other electronic format see DOI: 10.1039/b820060b

‡ Present address: Department of Chemistry, Purdue University, West Lafayette, IN 47907, USA.

Table 1 Crystal data and structure refinement for $[Rh_3(dpa)_4Cl_2][BF_4]\cdot 2CH_2Cl_2$ (**2**·$2CH_2Cl_2$)

	2·$2CH_2Cl_2$
Formula	$C_{42}H_{36}BCl_6F_4N_{12}Rh_3$
Fw	1317.07
T/K	150(2)
Crystal system	Monoclinic
Space group	$P2_1/n$
a/Å	11.3420(1)
b/Å	20.8203(2)
c/Å	20.3194(2)
α/°	90
β/°	93.6192(5)
γ/°	90
V/Å^3, Z	4788.73(8), 4
Reflections collected	36859
Independent reflections	10993
R_{int}	0.0529
R_F, R_{wF}^2 ($I > 2\sigma(I)$)[a]	0.0501, 0.0804
R_F, R_{wF}^2 (all data)[a]	0.1254, 0.1484

[a] $R_F = \sum|F_o - F_c|/\sum|F_o|$; $R_{wF}^2 = [\sum w|F_o^2 - F_c^2|^2/\sum wF_o^4]^{1/2}$.

Table 2 Selected bond distances (Å) and angles (°) observed for **1** and **2**

	1[b]	**2**
Rh–Rh[a]	2.392	2.363
Rh–Cl[a]	2.586	2.411
$Rh_{central}$–N[a]	2.014	2.010
$Rh_{terminal}$–N[a]	2.076	2.084
∠Rh–Rh–Rh	177.13	167.54

[a] Bond distances have been averaged. [b] From reference 3a.

geometry. The average Rh–Rh and Rh–Cl distances of **1** are 2.392 and 2.586 Å, respectively. The labeled ORTEP view of **2**, excluding solvent molecules, is displayed in Fig. 1. Structurally the oxidized compound **2** is very similar to **1**, except that the Rh–Rh–Rh unit in **2** significantly deviates from a linear arrangement (∠Rh(1)–Rh(2)–Rh(3) = 167.54°). The average Rh–Rh bond length of **2** is 2.363 Å, which is slightly shorter than that of **1**.[3a] Intuitively, it might be expected that an increase in the positive charge within the Rh_3 core upon oxidation would increase the repulsion between Rh atoms, which causes the elongated Rh–Rh bond distances. The shortening in the Rh–Rh distances from **1** to **2**, therefore, may indicate the enhancement of the Rh–Rh bond, which compensates for charge repulsion. The average Rh–Cl bond distance of **2** is 0.175 Å shorter than that of **1**. This variation can be explained as an increase of the attraction between the anionic Cl atoms and the cationic metallic framework. Another possible explanation of the structural changes might be the removal of an electron from the σ_{nb} Rh–Cl antibonding orbital upon oxidation, which resembles the structural features observed in the isoelectronic compound $Co_3(dpa)_4Cl_2$ (**3**).[4]

Magnetic and EPR measurements

Magnetic susceptibility measurements of **1** and **2** were made on a polycrystalline sample in the temperature range 4–300 K. The temperature dependence of the effective magnetic moment (μ_{eff}) of **1** and **2** are shown in Fig. 2. As previously reported, the μ_{eff} of **1** is *ca.* 1.76 μ_B at 300 K and remains constant down to low

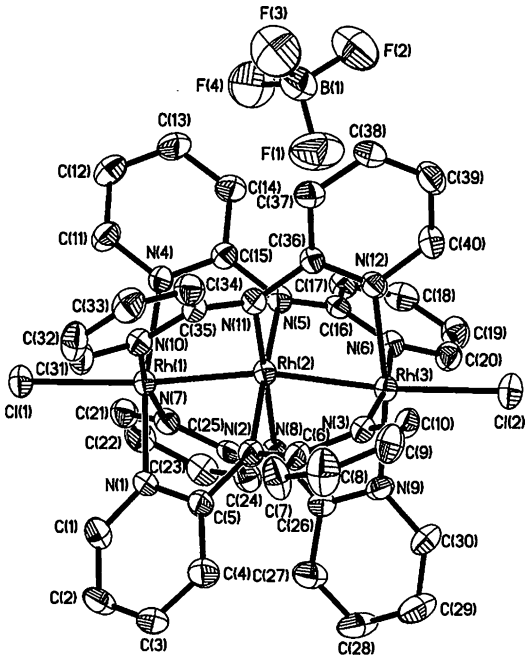

Fig. 1 ORTEP drawing of complex **2**. Thermal ellipsoids are drawn at the 30% probability level. Hydrogen atoms and interstitial solvents have been omitted for clarity.

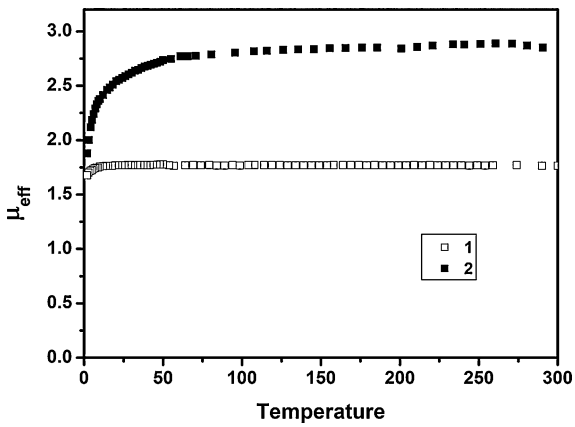

Fig. 2 Variation of magnetic susceptibility with temperature for compounds **1** and **2** at 2000 G applied field.

temperatures.[3a] This value indicates that compound **1** possesses one unpaired electron. The one-electron oxidized compound **2** displays a μ_{eff} value of 2.85 μ_B in the temperature range 50–300 K, which corresponds to the value of two unpaired electrons. At temperatures lower than 50 K, the μ_{eff} value decreases gradually due to relatively strong intermolecular interaction or zero-field splitting. It is clear that the increase of μ_{eff} upon oxidation would be expected to remove one β-spin electron of **1**. Such a characteristic is similar to that of the oxidative reaction of $[Co_3(dpa)_4Cl_2]$ (**3**).[4] An especially interesting observation is that neither complexes **1** nor **2** show spin-crossover as their isoelectronic family complexes **3** and **4** do.[4] Fig. 3 displays the powder EPR spectra obtained at 4 K for **1**. The sharp isotropic EPR signal centered at $g = 2.26$ is coincident with the feature of the doublet ground state.[4] For compound **2**, the EPR spectra recorded at 4 K is silent, which may indicate that the singlet or other states possess an even number of unpaired electrons.

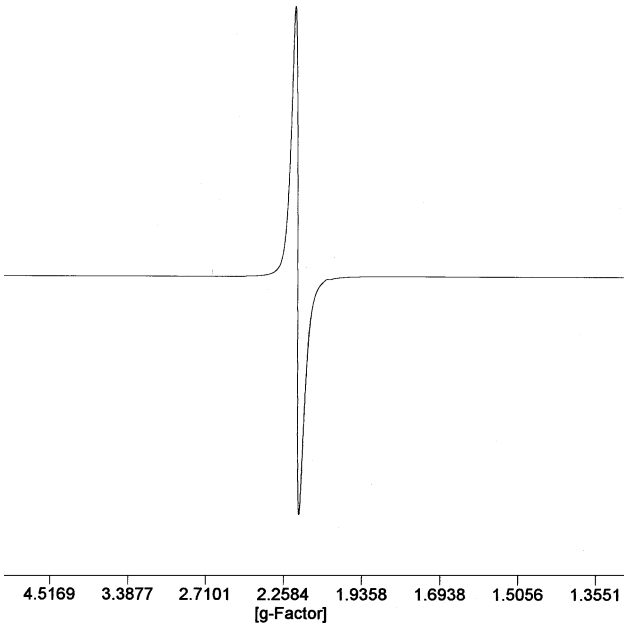

Fig. 3 EPR spectrum of compound **1** at 4 K.

Electrochemistry

Cyclic voltammetry of compound **1** in CH_2Cl_2 solution showed two reversible and one irreversible one-electron oxidation processes at potentials of 0.37, 1.02 and 1.53 V respectively (Fig. 4). No reversible reduction processes were observed. The first two oxidation processes are assigned to successive electron abstractions from **1**, leading to formation of $[Rh_3(dpa)_4Cl_2]^+$ (**2**) and $[Rh_3(dpa)_4Cl_2]^{2+}$. According to its low oxidative potential, compound **2** could be easily synthesized by using a chemical oxidant such as $FcBF_4$ in CH_2Cl_2. However, attempts to synthesize the two-electron oxidative complex, $[Rh_3(dpa)_4Cl_2]^{2+}$, using a variety of oxidants was unsuccessful.

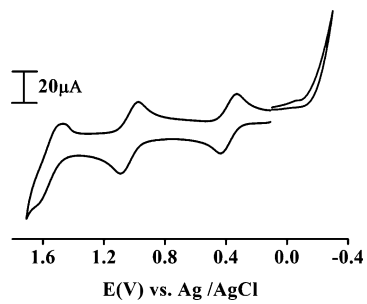

Fig. 4 The cyclic voltammogram of compound **1** in CH_2Cl_2 containing 0.1 M TBAP.

UV-Vis/NIR spectroelectrochemistry

Fig. 5 shows the spectral changes observed for compound **1** at applied potential from 0.23 to 0.53 V in CH_2Cl_2 containing 0.1 TMAP. The peaks at 315 and 460 nm decrease in intensity, while a new broad band at 1145 nm appears as the applied potential increases from +0.23 to +0.53 V. The resulting spectrum is identical to that of **2** obtained by a chemical method. Based on the spectral changes, the formation of a broad new band at 1145 nm is attributed to the inter-valence charge transfer (IVCT) transition. This IVCT band is a character of the electron delocalization within the mixed-valence complex **2**.[6]

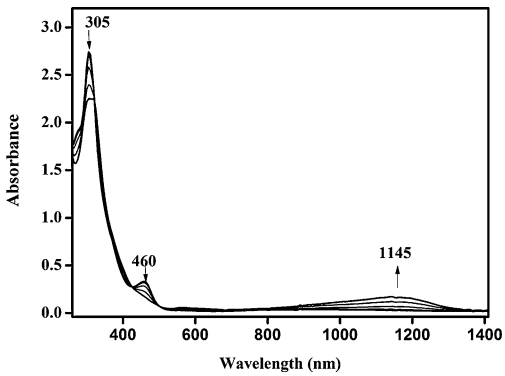

Fig. 5 Electronic absorption spectral changes for the first oxidation of compounds **1** in CH_2Cl_2 containing 0.1 M TBAP at various applied potentials from +0.23 to +0.53 V.

NMR spectra

The ^1H NMR spectra of compound **1** in CD_2Cl_2 and **2** in $CDCl_3$ are displayed in Fig. 6 and 7. Both spectra display four peaks with

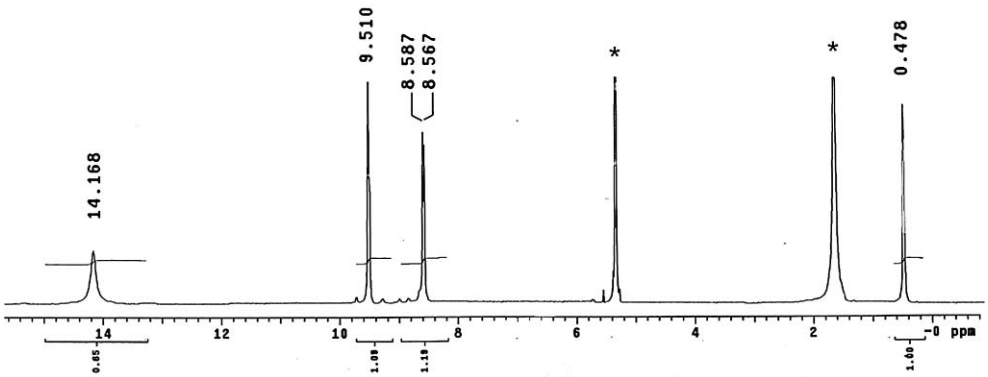

Fig. 6 ^1H NMR spectrum of **1** in CD_2Cl_2 at ambient temperature. Asterisks are solvent peaks.

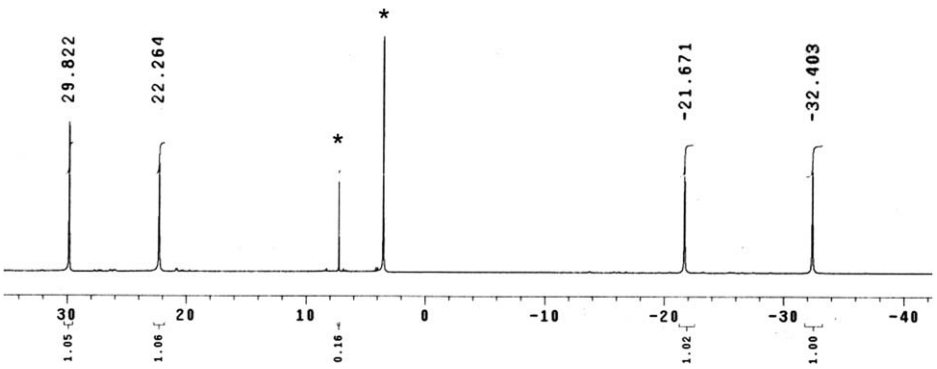

Fig. 7 ^{1}H NMR spectrum of **2** in $CDCl_3$ at ambient temperature. Asterisks are solvent peaks.

equal integration ratio. This appears to be consistent with the idealized D_4 symmetry assumed for both compounds. According to the DFT calculation (next section), the unpaired electrons of **1** occupy the σ non-bonding orbital which is mainly contributed from the d_{z^2} orbital of the terminal Rh atoms. The spin density of this unpaired electron will be donated to the proton mainly through space (*dipolar* interaction).[7] The contribution to the hyperfine shift is sometimes small, thus the changes of chemical shifts for the protons of **1** ($\delta = 14.17$, 9.51, 8.57 and 0.48 ppm) is not significant relative to the protons of the free ligand. The ^{1}H NMR spectrum of **2** clearly shows four signals at $\delta = 29.82$, 22.26, –21.67 and –32.40 ppm. The significant changes of the chemical shifts display the character of π contact shift as alternated peaks.[7] For **2**, one more unpaired electron may be qualitatively assigned to occupy in the δ antibonding orbital. Spin density of this unpaired electron is conveyed to the proton *via* the $d_{xy} - N_p$ pathway and induces significant down- or upfield shift for the protons of **2**.[7]

DFT calculations

To obtain further insight into the electronic structures of compounds **1** and **2**, a series of DFT calculations were performed. The geometries of compounds **1** and **2** were optimized in the idealized D_4 symmetry. The *z*-axis is assumed to be collinear with the Cl–Rh_3–Cl framework.

The geometry of **1** was fully optimized in the doublet ground state on the basis of the magnetic measure measurement and the optimized structural parameters are listed in Table 3. The electronic configuration ($e^4b_2^2a_2^1$) that gives rise to the $^2A_2$ state has been proposed to be the ground state of the isoelectronic compound **3**.[5] The calculated results of **1** show a similar electronic configuration ($^2A_2$), and the resulting optimized structural parameters are in good agreement with the crystal data. The qualitative MOs sequence of **1** is shown in Fig. 8. As proposed by Bénard and co-workers,[5b] the electrons occupying the π and δ orbital sets of the metal strings can be considered as localized on individual metal atoms and do not contribute to the metal–metal interaction. The unpaired electron of **1** occupies the σ non-bonding orbital (a_2) and with the doubly occupied σ bonding orbital generates a three-electrons-three-center bond. Therefore, the metal–metal bond of **1** is described as three σ electrons delocalized over the linear Rh_3 framework as that observed in **3**.

Table 3 Relevant geometrical parameters (distances in Å) and results computed for **1** in D_4 symmetry (basis set: BSI)

	Doublets			
	$^2A_2$	$^2E_2$	$^2B_2$	
	$e^4b_2^2a_2^1$	$e^3b_2^2a_2^2$	$e^4b_2^1a_2^2$	Expt.
Rh–Rh	2.438	2.413	2.451	2.392
Rh–Cl	2.523	2.634	2.685	2.586
Rh_{middle}–N	2.019	2.033	2.011	2.014
$Rh_{termial}$–N	2.107	2.108	2.087	2.076
ΔE/eV	0.000	0.248	0.185	
$<S^2>$	0.751	0.752	0.753	

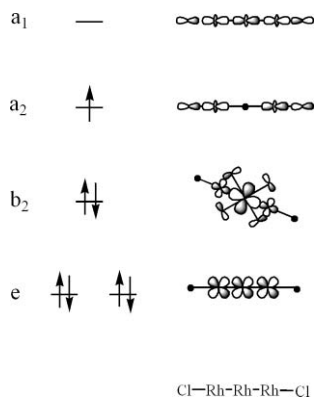

Fig. 8 Schematic molecular orbitals of **1** near the Fermi level.

The one-electron oxidative complex, **2**, shows the triplet ground state, indicating that the oxidation results in abstraction of one β-spin electron from **1**. The contraction of the crystal Rh–Cl distances upon oxidation is, therefore, due to the enhancement of charge attraction between Cl^- and the positive Rh_3 core, but not because of the removal of the electron from the singly occupied σ bonding orbital (a_2) (strong Rh–Cl antibonding character). On the basis of above assumption, the optimized structural parameters and relative energies of several possible electronic configurations of **2** are collected in Table 4. It is clear that the $^3B_1$ state ($e^4b_2^1a_2^1$) lies below 2^3E ($e^3b_2^2a_2^1$), 1^3E ($e^3b_2^1a_2^2$) and $^3A_1$ ($e^2b_2^2a_2^2$) states. The $^3B_1$ state, which resuls from the removal of the β-spin electron in the δ antibonding orbital (b_2) can be concluded to be the global minimal and the ground state. The magnitude of contraction of the optimized Rh–Cl distance (–0.0255 Å) upon oxidation is smaller

Table 4 Relevant geometrical parameters (distances in Å) and results computed for **2** in D_4 symmetry (basis set: BSI, functional: BP86)

	Singlet		Triplet				
	$^1A_1$	$^1B_1$[a]	$^3B_1$	1^3E	2^3E	$^3A_1$	
	$e^4b_2{}^2a_2{}^0$	$e^4b_2{}^1a_2{}^1$	$e^4b_2{}^1a_2{}^1$	$e^3b_2{}^1a_2{}^2$	$e^3b_2{}^2a_2{}^1$	$e^2b_2{}^2a_2{}^2$	Expt.
Rh–Rh	2.434	2.439	2.439	2.427	2.407	2.395	2.363
Rh–Cl	2.399	2.497	2.497	2.577	2.468	2.547	2.411
Rh_{middle}–N	2.011	2.007	2.008	2.014	2.025	2.033	2.010
$Rh_{termial}$–N	2.113	2.101	2.101	2.104	2.112	2.117	2.084
ΔE/eV	0.224	0.022	0.000	0.470	0.266	0.613	
$<S^2>$	0	1.006	2.005	2.005	2.004	2.004	

[a] Broken symmetry state.

than that observed in the crystal structure (–0.175 Å). Attempts using several different basis sets and functionals to improve the deviation of calculated Rh–Cl bond lengths were unsuccessful (ESI†). The discrepancy in experimental and calculated Rh–Cl distances, therefore, may be attributed to the crystal packing force or the significant distortion of the metal framework of the crystal structure (∠Rh(1)–Rh(2)–Rh(3) = 167.54°).

An excellent description for the singlet/triplet spin-crossover of $[Co_3(dpa)_4Cl_2]^+$ (**4**) previously reported by McGrady and co-workers involves the presence of an open-shell singlet state ($^1B_1$).[5] The $^1B_1$ state arises from the reversal of spin in a_2 or b_2 orbitals (Scheme 1). Because the $^1B_1$ state of **4** is structurally and energetically ($\Delta E = 0$ eV) identical to the $^3B_1$ state, it was proposed that these two states take part in the singlet/triplet spin crossover. For $[Rh_3(dpa)_4Cl_2]^+$ (**2**), it may seem surprising that the $^1B_1$ state lies 0.0219 eV above the $^3B_1$ (Table 4). Because of this energy barrier, the corresponding spin-crossover of **2** does not occur in the observed magnetic measurements.

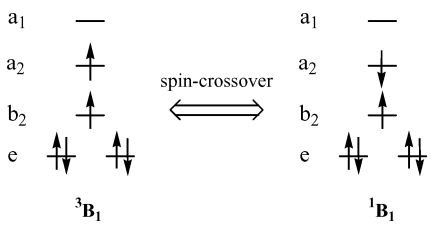

Scheme 1

Conclusions

The physical properties of trirhodium complexes, $[Rh_3(dpa)_4Cl_2]$ (**1**) and $[Rh_3(dpa)_4(Cl)_2](BF_4)$ (**2**), have been extensively studied in this work. The magnetic measurements show that **1** and **2** exhibit S = doublet and triplet ground states. DFT calculations confirm the ground states of **1** ($^2A_2$) and **2** ($^3B_1$), consistent with the magnetic measurements. Theoretical calculations also suggest that the chemical oxidation of **1** involves removal of the electron in the δ antibonding orbital (b_2) (Fig. 8), which is in agreement with the contracted crystal structural Rh_{middle}–N bond distances upon oxidation. In contrast to the magnetic properties of their isoelectronic analogues, $[Co_3(dpa)_4Cl_2]$ (**3**) and $[Co_3(dpa)_4(Cl)_2]^+$ (**4**), the spin-crossover phenomena were not observed for **1** and **2**, that may be attributed to the larger energy gap between $^3B_1$ and open-shell singlet $^1B_1$ states. Finally, the qualitative explanations of the ^1H NMR spectra of **1** and **2** support these calculated electronic configurations.

Experimental

Materials

All reagents and solvents were purchased from commercial sources and were used as received unless otherwise noted. CH_2Cl_2 used for electrochemistry was dried over CaH_2 and freshly distilled prior to use. Tetra-*n*-butylammonium perchlorate (TBAP) was recrystallized twice from ethyl acetate and dried under vacuum.

Physical measurements

Absorption spectra were performed on a Shimadzu UV-3600 spectrophotometer. IR spectra were obtained from a Nicolet Fourier-Transform in the range 500–4000 cm^{-1}. FAB mass spectra were taken on a JEOL HX-110 HF double-focusing spectrometer operating in the positive ion detection mode. Magnetic susceptibility was collected by a Quantum external magnetic field 2000 G. Electrochemistry was carried out on a CH Instruments, (Model 750A) using CH_2Cl_2 solvent with 0.1 M TBAP and 1 mM analytes. Cyclic voltammetry was recorded with a homemade three-electrode cell equipped with a BAS glassy carbon (0.07 cm^2) disk as the working electrode, a platinum wire as the auxiliary electrode, and a home-made Ag/AgCl (saturated) reference electrode. The reference electrode is separated from the bulk solution by a double junction filled with electrolyte solution. Potentials are reported *vs.* Ag/AgCl (saturated) and referenced to the ferrocene–ferrocenium ($[Cp_2Fe]/[Cp_2Fe]^+$) couple which occurs at $E_{1/2} = +0.54$ V *vs.* Ag/AgCl (saturated). The working electrode was polished with 0.3 μm alumina on Buehler felt pads and was subjected to ultrasound for 1 min prior to each experiment. The reproducibility of individual potential values was within ±5 mV. Optically transparent thin-layer electrochemical electrode (OTTLE) spectra were accomplished with the use of a 1 mm thick UV cell, a 100-mesh platinum gauze as working electrode, a platinum wire as auxiliary electrode, and a Ag/AgCl (saturated) reference electrode.

X-Ray crystallographic determinations

The crystals were mounted on a glass fiber. Crystal data were collected on a NONIUS Kappa CCD diffractometer with monochromatized Mo Kα radiation ($\lambda = 0.71073$ Å) at $T = 150(2)$ K. Cell parameters were retrieved and refined using *DENZOSMN* software on all observed reflections. Data reduction was performed with the *DENZO-SMN* software.[8] An empirical absorption was based on the symmetry-equivalent reflections and absorption corrections were applied with the SORTAV program.[8] All the structures were solved by using the *SHELXS-97* and refined with *SHELXL-97* by full-matrix least squares on F^2 values.[8] Hydrogen atoms were fixed at calculated positions and refined using a riding mode.

CCDC reference number 708776.

Syntheses

$[Rh_3(dpa)_4Cl_2]$ (1). This compound was prepared according to the literature procedures. A mixture of Hdpa (171 mg, 1 mmol), $Rh_2(OAc)_4$ (214 mg, 0.48 mmol) and naphthalene (20 g) were stirred at 160 °C for 1 h under argon atmosphere and then *t*BuOK (112 mg) in *n*BuOH (2 ml) was added slowly into the mixture. After 20 min, 100 mg LiCl was added to this solution for further 20 min. The solution was cooled and then washed with excess hexane to remove naphthalene. The crude product was extracted with 50 ml CH_2Cl_2. The solution was condensed and layered with hexane. The dark brown crystals formed after two weeks. Yield: 8%. Mass spectrum: m/z 1060 (M^+). UV-VIS/near-IR : 305 nm (31.5×10^3) 460 nm (2.77×10^3), IR(KBr) : 1599, 1588, 1541, 1460 and 1420 cm^{-1}. ^{1}H-NMR (400 MHz; CD_2Cl_2): δ (ppm) 0.478 (4 H), 8.577 (4 H), 9.510 (4 H), 14.168 (4H).

$[Rh_3(dpa)_4Cl_2](BF_4)$ (2). To a solution of compound **1** (50 mg, 0.05 mmol) in a mixture of CH_2Cl_2 (25 mL) and MeOH (1 mL) was added $[Cp_2Fe](BF_4)$ (18.6 mg, 0.06 mmol) under argon atmosphere. The resulting solution turned to dark green immediately. After stirring for 30 min, the solution was filtered. The solvent was evaporated under vacuum. The residual was dissolved in CH_2Cl_2 and recrystallized with diethyl ether. The dark-green thin plate crystals were obtained by layering the CH_2Cl_2 solution containing the compound with hexane. Yield: 82%. Mass spectrum: m/z 1060 (M^+). UV-VIS/near-IR : 320 nm (5.97×10^3) 1145 nm (7.4×10^3), IR(KBr) : 1600, 1589, 1542, 1461 and 1420 cm^{-1}. ^{1}H-NMR (400 MHz; $CDCl_3$): δ (ppm) –32.403 (4 H), –21.671 (4 H), 22.264 (4 H), 29.822 (4H).

Computational methods

Calculations and geometry optimisations reported in this article have been done by density-functional theory (DFT) methods[9] using the ADF 2006.01 program package.[10] All calculations employed the spin-unrestricted approach and were done at the GGA level (Vosko–Wilk–Nusair (VWN) for local density approximation[11]) with the BP86[12] and with the PW91[13] exchange–correlation functionals. Full geometry optimizations were done within the idealize D_4 symmetry constrains for $[Rh_3(dpa)_4Cl_2]$ (**1**) and $[Rh_3(dpa)_4(Cl)_2]^+$ (**2**). Within the ADF program slater type orbitals (STO) with the two basis sets, referred to as BSI and BSII, were used. In BSI, double-ζ quality for H, double-ζ quality with polarization function for C, N, Cl and triple-ζ quality with polarization function for Rh. The inner shells were treated within the frozen-core approximation (1 s for C and N, 1s–2p for Cl, 1s–3d for Rh). In BS II, double-ζ quality for H, double-ζ quality with polarization function for C, N, Cl and triple-ζ quality with polarization function for Rh. The inner shells were treated within the frozen-core approximation (1 s for C and N).

Acknowledgements

We acknowledge the National Science Council and the Ministry of Education of Taiwan for financial support. We are pleased to thank Prof. M. Bénard, Prof. M.-M. Rohmer (Université Louis Pasteur, France), and Prof. J. E. McGrady (University of Glasgow, UK) for their practical discussions. We wish to express our gratitude to Prof. R.-J. Chen (National Chung Hsing University, Taiwan) for kindly providing the computing resource.

References

1 (*a*) F. A. Cotton, L. M. Daniels, T. Lu, C. A. Murillo and X. Wang, *J. Chem. Soc., Dalton Trans.*, 1999, 517; (*b*) J. F. Berry, F. A. Cotton, P. Lei, T. Lu and C. A. Murillo, *Inorg. Chem.*, 2003, **42**, 3534; (*c*) L.-G. Zhu and S.-M. Peng, *Wuji Huaxue Xuebao*, 2002, **18**, 117; (*d*) J. K. Bera and K. R. Dunbar, *Angew. Chem., Int. Ed.*, 2002, **41**, 4453.

2 (*a*) J. F. Berry, in *Multiple Bonds between Metal Atoms*, 3rd ed.; F. A. Cotton, C. A. Murillo, R. A. Walton, Eds; Springer-Science and Business Media, Inc., New-York, 2005; (*b*) C.-Y. Yeh, C.-C. Wang, C.-h. Chen and S.-M. Peng, in *Nano Redox Sites: Nano-Space Control and its Applications*, T. Hirao, Ed.; Springer, Berlin, 2006, Chapter 5, pp. 85–117; (*c*) S. Aduldecha and B. Hathaway, *J. Chem. Soc., Dalton Trans.*, 1991, 993; (*d*) E.-C. Yang, M.-C. Cheng, M.-S. Tsai and S.-M. Peng, *J. Chem. Soc., Chem. Commun.*, 1994, 2377; (*e*) R. Clérac, F. A. Cotton, L. M. Daniels, K. R. Dunbar, C. A. Murillo and X. Wang, *J. Am. Chem. Soc.*, 2001, **123**, 1256; (*f*) L.-P. Wu, P. Field, T. Morrissey, C. Murphy, P. Nagle, B. Hathaway, C. Simmons and P. Thornton, *J. Chem. Soc., Dalton Trans.*, 1990, 3835; (*g*) S.-J. Shieh, C.-C. Chou, G.-H. Lee, C.-C. Wang and S.-M. Peng, *Angew. Chem., Int. Ed. Engl.*, 1997, **36**, 56; (*h*) C.-Y. Yeh, C.-H. Chou, K.-C. Pan, C.-C. Wang, G.-H. Lee, Y.-O. Su and S.-M. Peng, *J. Chem. Soc., Dalton Trans.*, 2002, 2670; (*i*) H.-C. Chang, J.-T. Li, C.-C. Wang, T.-W. Lin, H.-C. Lee, G.-H. Lee and S.-M. Peng, *Eur. J. Inorg. Chem.*, 1999, 1243; (*j*) F. A. Cotton, L. M. Daniels, T. Lu, C. A. Murillo and X. Wang, *J. Chem. Soc., Dalton Trans.*, 1999, 517; (*k*) I. P.-C. Liu, M. Bénard, H. Hasanov, I.-W. P. Chen, W.-H. Tseng, M.-D. Fu, M.-M. Rohmer, C.-h. Chen, G.-H. Lee and S.-M. Peng, *Chem.–Eur. J.*, 2007, **13**, 8667; (*l*) C.-H. Chien, J.-C. Chang, C.-Y. Yeh, L.-M. Fang, Y. Song and S.-M. Peng, *Dalton Trans.*, 2006, 3249; (*m*) S.-Y. Lai, T.-W. Lin, Y.-H. Chen, C.-C. Wang, G.-H. Lee, M. Yang, M. Leung and S.-M. Peng, *J. Am. Chem. Soc.*, 1999, **121**, 250; (*n*) Y.-H. Chen, C.-C. Lee, C.-C. Wang, G.-H. Lee, S.-Y. Lai, F.-Y. Li, C.-Y. Mou and S.-M. Peng, *Chem. Commun.*, 1999, 1667; (*o*) H. Hasanov, U.-K. Tan, G.-H. Lee and S.-M. Peng, *Inorg. Chem. Commun.*, 2007, **10**, 983; (*p*) S.-M. Peng, C.-C. Wang, Y.-L. Jang, Y.-H. Chen, F.-Y. Li, C.-Y. Mou and M.-K. Leung, *J. Magn. Magn. Mater.*, 2000, **209**, 80.

3 (*a*) J.-T. Sheu, C.-C. Lin, I. Chao, C.-C. Wang and S.-M. Peng, *Chem. Commun.*, 1996, 315; (*b*) C.-K. Kuo, I. P.-C. Liu, C.-Y. Yeh, C.-H. Chou, T.-B. Tsao, G.-H. Lee and S.-M. Peng, *Chem.–Eur. J.*, 2007, **13**, 1442; (*c*) M.-M. Rohmer, I. P.-C. Liu, J.-C. Lin, M.-J. Chiu, G.-H. Lee, M. Bénard, X. López and S.-M. Peng, *Angew. Chem., Int. Ed.*, 2007, **46**, 3533; (*d*) I. P.-C. Liu, G.-H. Lee, S.-M. Peng, M. Bénard and M.-M. Rohmer, *Inorg. Chem.*, 2007, **46**, 9602; (*e*) G.-C. Huang, M. Bénard, M.-M. Rohmer, L.-A. Li, M.-J. Chiu, C.-Y. Yeh, G.-H. Lee and S.-M. Peng, *Eur. J. Inorg. Chem.*, 2008, **11**, 1767; (*f*) C. Yin, G.-C. Huang, C.-K. Kuo, M.-D. Fu, H.-C. Lu, J.-H. Ke, K.-N. Shih, Y.-L. Huang, G.-H. Lee, C.-Y. Yeh, C.-h. Chen and S.-M. Peng, *J. Am. Chem. Soc.*, 2008, **130**, 10090; (*g*) M. Nippe, E. Victor and J. F. Berry, *Eur. J. Inorg. Chem.*, 2008, **36**, 5569.

4 (*a*) R. Clérac, F. A. Cotton, K. R. Dunbar, T. B. Lu, C. A. Murillo and X. Wang, *J. Am. Chem. Soc.*, 2000, **122**, 2272; (*b*) J. F. Berry,

F. A. Cotton, L. M. Daniels, C. A. Murillo and X. Wang, *Inorg. Chem.*, 2003, **42**, 2418.
5 (*a*) D. A. Pantazis, C. A. Murillo and J. E. McGrady, *J. Am. Chem. Soc.*, 2006, **128**, 4128; (*b*) M.-M. Rohmer and M. Bénard, *J. Am. Chem. Soc.*, 1998, **120**, 9372; (*c*) M.-M. Rohmer and Bénard, *Chem. Soc. Rev.*, 2001, **30**, 340; (*d*) D. A. Pantazis, C. A. Murillo and J. E. McGrady, *Dalton Trans.*, 2008, 608.
6 *Mixed Valence Compounds*, ed. D. M. Brown, D. Reidel, Dordrecht, Holland, 1980.
7 (*a*) I. Bertini, P. Turano and A. J. Vila, *Chem. Rev.*, 1993, **93**, 2833; (*b*) I. Bertini, and C. Luchinat, *NMR of Paramagnetic Molecules in Biological Systems*, Benjamin/Cummings, Menlo Park CA, 1986; (*c*) I. Bertini, C. Luchinat, and G. Parigi, *Solution NMR of Paramagnetic Molecules*, Elsevier, Amsterdam, 2001.
8 (*a*) Z. Otwinowski and W. Minor, *Methods Enzymol.*, 1997, **276**, 307; (*b*) R. H. Blessing, *Acta Crystallogr. Sect. A*, 1995, **51**, 33; (*c*) G. M. Sheldrick, *Acta Crystallogr. Sect. A*, 1990, **46**, 467; (*d*) G. M. Sheldrick, *SHELXL-97*, University of Gőttingen, Germany, 1997.
9 R. G. Parr, and W. Yang, *Density Functional Theory of Atoms and Molecules*, Oxford University Press: New York, 1989.
10 E. J. Baerends, *et al. ADF 2006.01 SCM; Theoretical Chemistry*, Vrije Universiteit, Amsterdam, The Netherlands; http://www.scm.com.
11 S. H. Vosko, L. Wilk and M. Nusair, *Can. J. Phys.*, 1980, **58**, 1200.
12 (*a*) A. D. Becke, *Phys. Rev.*, 1988, **388**, 3098; (*b*) J. P. Perdew, *Phys. Rev.*, 1986, **33**, 8822.
13 J. P. Perdew, J. A. Chekavry, S. H. Vosko, K. A. Jackson, M. R. Perderson, D. J. Singh and C. Fioihais, *Phys. Rev. B*, 1992, **46**, 6671.